香港浸會大學
HONG KONG BAPTIST UNIVERSITY

HKBU Scholars

Visible-blind near-infrared organic photodetectors

Wang, Zhuangmiao; Tang, Yu; Han, Jiayin; Zhu, Furong

Published in:
Applied Physics Letters

DOI:
10.1063/5.0180711

Published: 08/01/2024

Document Version:
Peer reviewed version

Link to publication

Citation for published version (APA):
Wang, Z., Tang, Y., Han, J., & Zhu, F. (2024). Visible-blind near-infrared organic photodetectors. *Applied Physics Letters*, *124*(2), Article 021103. https://doi.org/10.1063/5.0180711

General rights
Copyright and intellectual property rights for the publications made accessible in HKBU Scholars are retained by the authors and/or other copyright owners. In addition to the restrictions prescribed by the Copyright Ordinance of Hong Kong, all users and readers must also observe the following terms of use:

- Users may download and print one copy of any publication from HKBU Scholars for the purpose of private study or research
- Users cannot further distribute the material or use it for any profit-making activity or commercial gain
- To share publications in HKBU Scholars with others, users are welcome to freely distribute the permanent publication URLs

Downloaded on: 07 Dec, 2024

Visible-Blind near-infrared organic photodetectors

Zhuangmiao Wang, Yu Tang, Jiayin Han and Furong Zhu[a)]

Department of Physics, Research Centre of Excellence for Organic Electronics, Institute of Advanced Materials, Hong Kong Baptist University, Kowloon Tong, Hong Kong, China

[a)]Author to whom correspondence should be addressed: frzhu@hkbu.edu.hk

The presently available commercial photodetectors have a broadband photoresponse and require different external optical filters to block the undesired light outside the detection spectrum window, e.g., near-infrared (NIR) detection. The use of an NIR bandpass has technical limitations in curved or flexible large-area photodetectors, as an NIR bandpass depends critically on the difference in the interference of the optical path in the filter. This work reports the effort to develop a high-performance filter-free organic photodetector (OPD) with a double bulk heterojunction (BHJ) structure. The visible-blind NIR photodetection is realized by eliminating the photocurrent generated in the front visible light-absorbing BHJ optical depletion layer, due to the suppression of electron transport by incorporating a copper thiocyanate-based electron-blocking layer in the OPD. Only excitons generated in the rear NIR-absorbing BHJ contribute to photocurrent in the OPD, thereby achieving visible-blind NIR photodetection. The double BHJ OPD has a high responsivity of 0.38 A/W at 1050 nm and a specific detectivity of $>10^{13}$ Jones over the wavelength range from 800 to 1050 nm, making it an ideal candidate for applications in optical communication, food quality detection, wellness monitoring, and NIR image sensors.

Detection of near-infrared (NIR) electromagnetic waves is often accomplished by incorporating a broadband photodetector with an external NIR bandpass filter. However, the utilization of an external NIR bandpass filter reduces the overall photoresponsivity, adding in additional device integration complexity and manufacturing cost. Organic photodetectors (OPDs) are promising optical detection technology compared to conventional inorganic semiconductor-based photodetectors, due to their cost effectiveness and broad range of applications. Despite their flexible design with small molecules, polymer/nonfullerene acceptor and hybrid small molecule/polymer blends, OPDs are generally broadband photodetectors due to the nature of broadband absorption behavior. Realizing visible-blind NIR OPD with a high detectivity is very attractive for different applications.[1] Various approaches have been reported for developing filter-free OPDs, including microcavity,[2,3] charge-collection narrowing (CCN),[4,5] charge injection narrowing,[6,7] self-filtering,[8–10] and bias switchable dual-band photodetection techniques.[11,12] The use of microcavity OPDs enables to realize narrowband photoresponse, however having a crosstalk issue arising from the resonance interference of the adjacent wavelengths.[2,13] CCN-type OPDs require a relatively thick photoactive layer of >2 μm, which leads to a reduction in the photodetection efficiency, caused by the loss of the photogenerated charges in the thick photoactive layer.[4] The charge injection narrowing approach helps to amplify the low photoresponse of CCN-type OPDs through photomultiplication effect, however it requires a high applied voltage.[7]

In a previous study, a filter-free visible-blind NIR OPD comprising a pristine poly[4,8-bis(5-(2-ethylhexyl)thiophen-2-yl)benzo[1,2-b;4,5-b’] dithiophene-2,6-diyl-alt-(4-(2-ethylhexyl)-3-fluorothieno[3,4-b] thiophene-)-2-carboxylate-2-6-diyl)] (PTB7-Th) polymer optical depletion layer and a rear NIR absorber has been reported.[14] The front pristine PTB7-Th polymer optical depletion layer in the filter-free visible-blind NIR OPD absorbs the visible light portion of the incoming electromagnetic waves, while the rear bulk heterojunction (BHJ) responses to the NIR portion of the incoming electromagnetic waves. However, the detectivity of the filter-free

visible-blind NIR NIR OPD with a pristine PTB7-Th polymer optical depletion layer is limited due to the relative high noise current. Mitigating the noise current is one of the key technical developments to enhance the performance of OPDs.

This work reports the effort to develop a high-performance visible-blind NIR OPD, comprising a layer configuration of visible-absorbing BHJ/copper thiocyanate (CuSCN)-based electron-blocking layer (EBL)/NIR-absorbing BHJ. The double BHJ OPDs have a noise spectral density of 8.0×10^{-15} A $Hz^{-1/2}$, which is more than two orders of magnitude lower than that of a control OPD with a pristine PTB7-Th polymer optical depletion layer (1.4×10^{-12} A $Hz^{-1/2}$), leading to a high specific detectivity (D^*) of $>10^{13}$ Jones over the wavelength range from 800 to 1050 nm and a responsivity, $R(\lambda)$, of 0.38 A/W at 1050 nm.

The visible-blind NIR OPDs have a layer configuration of indium tin oxide (ITO)/poly(3,4-ethylenedioxythiophene):poly(styrenesulfonate) (PEDOT:PSS) hole-transporting layer (HTL) (30 nm)/optical depletion layer/CuSCN EBL/NIR-absorbing BHJ layer/ZnO (10 nm)/Ag (100 nm). The binary PTB7-Th:[6,6]-phenyl-C71-butyric acid methyl ester ($PC_{71}BM$) (1:1) BHJ and the pristine PTB7-Th polymer optical depletion layers were prepared by spin-coating method. The mixture solution of PTB7-Th:2,2'-((2Z,2'Z)-((5,5'- (4,4-bis(2- ethylhexyl)-4H-cyclopenta[1,2-b:5,4-b']dithiophene-2,6-diyl)bis(4-((2-ethylhexyl)oxy) thiophene-5,2-diyl)) bis(methanylylidene)) bis(5,6-difluoro3-oxo-2,3-dihydro-1H-indene-2,1-diylidene)) dimalononi-trile (COTIC-4F): (2,20-((2Z,20Z)-((12,13-bis(2-ethylhexyl)-3,9-diundecyl-12,13-dihydro-[1,2,5] thiadiazolo[3, 4-e]thieno[2", 30':4',50]thieno[20,30:4,5] pyrrolo[3,2-g]thieno[20,30:4,5]thieno[3,2-b]ind-ole-2,10-diyl)bis (me-thanylylidene))bis(5,6-difluoro-3-oxo-2,3-dihydro-1H-indene-2,1-diylidene))dima-lononitrile) (Y6) with a weight ratio of PTB7-Th to COTIC-4F to Y6 of 1:1.05:0.45, dissolved in chlorobenzene, was formulated for preparation of the ternary BHJ active layer. A 100 nm thick ternary PTB7-Th:COTIC-4F:Y6 NIR absorbing BHJ layer was first spin-coated on the precleaned Si wafer and then it was removed from Si wafer and formed on the surface of glass/ITO/PEDOT:PSS/PTB7-Th/CuSCN

and glass/ITO/PEDOT:PSS/PTB7-Th:$PC_{71}BM$/CuSCN using a transfer process.[14] The OPDs have an active area of 3.0 × 3.0 mm^2, defined by the overlap area of the front ITO and rear Ag contacts.

Noise current in NIR OPDs is closely associated with the interfacial properties, material properties, device structure and process conditions.[15-18] The cross-sectional view of the visible-blind NIR OPD, having an optical depletion layer, e.g., a pristine PTB7-Th polymer layer and a binary PTB7-Th:$PC_{71}BM$ BHJ, and a rear ternary PTB7-Th:COTIC-4F:Y6 BHJ NIR absorber, is shown in Fig. 1(a). The visible-blind NIR OPD comprises a layer configuration of ITO/PEDOT:PSS HTL/optical depletion layer/CuSCN EBL/PTB7-Th:COTIC-4F:Y6/ZnO electron-transporting layer (ETL)/Ag. The normalized absorption spectra measured for the thin films of $PC_{71}BM$, PTB7-Th, PTB7-Th:$PC_{71}BM$ and PTB7-Th:COTIC-4F:Y6 are shown in Fig. 1(b). The results show that there is an overlap in the absorption spectra below the wavelength, λ, of 750 nm, measured for the ternary PTB7-Th:COTIC-4F:Y6 and binary PTB7-Th:$PC_{71}BM$ blend layers. The structure of the multilayer OPD, with a double BHJ of PTB7-Th:$PC_{71}BM$/CuSCN EBL/PTB7-Th:COTIC-4F:Y6, is optimized such that the visible part of the incoming electromagnetic waves with λ <750 nm is fully absorbed by the front binary PTB7-Th:$PC_{71}BM$ BHJ, whereas the long wavelength portion of the incoming light with λ >750 nm is absorbed by the rear ternary PTB7-Th:COTIC-4F:Y6 BHJ. The visible-blind NIR photodetection can then be realized by eliminating the photocurrent generated in the front PTB7-Th:$PC_{71}BM$ BHJ, acting as an optical depletion layer, in the double BHJ OPD operated at a reverse bias. Only excitons generated in the rear PTB7-Th:COTIC-4F:Y6 BHJ in the OPD, due to its absorption of photons with λ >750 nm, contribute to photocurrent, thereby achieving visible-blind NIR photodetection.

$R(\lambda)$ of an OPD is calculated using the ratio of the photocurrent to the power of incident light as a function of the wavelength:

$$R(\lambda) = \frac{J_{ph}(\lambda)}{P_{light}} = \frac{J_{light}(\lambda) - J_{dark}}{P_{light}}, \quad (1)$$

where $J_{ph}(\lambda)$ is the photocurrent generated by the OPD, $J_{light}(\lambda)$ is the current of the photodetectors under the illumination of light, J_{dark} is the dark current, and P_{light} is the power of the incoming light. $R(\lambda)$ of a double BHJ OPD has a typical visible-blind NIR photoresponse behavior over the wavelength range from 750 to 1100 nm, as shown in Fig. 1(c). The incoming light with λ <750 nm absorbed by the front BHJ optical depletion layer does not generate any observable photocurrent. The double BHJ OPD, operated without bias, has a peak responsivity of 0.38 A/W at 1050 nm, which is much higher than that of a control OPD at 1050 nm (0.22 A/W). The double BHJ OPD has a much higher responsivity as compared to that of a commercial Si-based photodetector at long wavelength of >1000 nm.

The double BHJ OPD also has a low crosstalk over different spectral regions, which can be described using the spectral rejection ratio (*SRR*), defined as the ratio of $R(\lambda_{\text{target}})$ at the target wavelength to $R(\lambda_{\text{ref}})$ at the untargeted reference wavelength range:[14]

$$SRR(\lambda_{target}, \lambda_{ref}) = \frac{R(\lambda_{target})}{R(\lambda_{ref})}. \quad (2)$$

As shown in Fig. 1(c), $R(\lambda)$ measured for the double BHJ OPD at 1050 nm is 0.38 A/W, which is more than two orders of magnitude higher than its $R(\lambda)$ at 550 nm (0.0013 A/W). According to Eq. (2), it results an *SRR*(1050 nm, 550 nm) of >290, revealing a low crosstalk over NIR and visible spectral regions, enabling a filter-free NIR detection technology that blocks away visible light. The schematic energy levels of the functional materials used in the double BHJ OPD and the control OPD are shown in Fig. 1(d). The molecular structures of the functional materials used in the work are shown in Fig. S1 of the supplementary material.

Noise spectral density, S_n, measured for a visible-blind OPD with a 700 nm thick front PTB7-Th:$PC_{71}BM$ BHJ optical depletion layer and a control OPD with an 800 nm thick pristine PTB7-Th polymer optical depletion layer are shown in Fig. 2(a). An S_n of 8.0×10^{-15} A $Hz^{-1/2}$ was obtained for a double BHJ OPD, which is about two orders of magnitude lower than that of a control OPD (1.4×10^{-12} A $Hz^{-1/2}$). The results suggest that a double BHJ OPD is more effective

in mitigating the noise current as compared to that in a control OPD.

D^* of an OPD is wavelength dependent which is related to $R(\lambda)$ and S_n:

$$D^* = \frac{\sqrt{A} \times R(\lambda)}{S_n}, \tag{3}$$

where A is the OPD active area. D^* of $>10^{13}$ Jones over the wavelength range from 800 to 1050 nm was obtained for a double BHJ OPD operated at -0.1 V, as shown in Fig. 2(b). D^* is associated closely with the noise current, which is one of the main factors responsible for the detectivity in the NIR OPDs. The performance of a double BHJ OPD is apparently more favorable as compared to that of a control OPD. D^* of $>10^{13}$ Jones over the NIR wavelength range is obtained for a double BHJ OPD, which is more than two orders of magnitude higher than that of a control OPD (5.0×10^{10} Jones), as shown in Fig. S2 of the supplementary material.

The profiles of optical field distribution and absorbed photon distribution in a double BHJ OPD, with a layer configuration of ITO/PEDOT:PSS (30 nm)/PTB7-Th:$PC_{71}BM$ (700 nm)/CuSCN (60 nm)/PTB7-Th:COTIC-4F:Y6 (100 nm)/ZnO (10 nm)Ag (100 nm), over the wavelength range from 400 to 1100 nm were analyzed using optical admittance analysis,[11] as shown in Figs. 3(a) and 3(b). Wavelength-dependent refractive indexes, $n(\lambda)$, and extinction coefficients, $k(\lambda)$, measured for the PTB7-Th layer, binary PTB7-Th: $PC_{71}BM$ (1:1) BHJ layer, ternary PTB7-Th:COTIC-4F:Y6 (1:1.05:0.45) BHJ and CuSCN layer, used for the simulation in this work are shown in Fig. S3 of the supplementary material. The optical simulation reveals that short wavelength part of the incoming light, e.g., visible light with λ <750 nm, is entirely absorbed by the 700 nm thick front PTB7-Th:$PC_{71}BM$ BHJ, while the long wavelength part of the incoming light with λ >750 nm is fully absorbed by the rear PTB7-Th:COTIC-4F:Y6 BHJ. The 700 nm thick PTB7-Th:$PC_{71}BM$ BHJ layer acts as an optical depletion layer to filter out the visible light, allowing the long-wavelength light to reach the rear ternary PTB7-Th:COTIC-4F:Y6 BHJ layer. Optical field distribution and absorbed photon distribution calculated for a double BHJ OPD at two different wavelengths of 500 and 1050 nm are shown in Figs. 3(c) and

3(d). The distribution profiles of the optical field and absorbed photons calculated for a control OPD at 500 and 1050 nm are shown in Fig. S4 of the supplementary material.

Compared to a control OPD, there is a sizeable interfacial energy barrier at the $PC_{71}BM$/CuSCN EBL interface in a double BHJ OPD, formed due to a large mismatch in the highest occupied molecular orbital level between $PC_{71}BM$ donor and CuSCN EBL, as shown in Fig. 4(a). This mismatch induces an interfacial energy barrier for holes, leading to a space charge accumulation at the $PC_{71}BM$/CuSCN interface. The charge accumulation behavior in a double BHJ OPD was analyzed using current density–voltage (*J–V*) characteristics measured for the hole-only devices of ITO/PEDOT:PSS/PTB7-Th:$PC_{71}BM$/CuSCN/Ag and ITO/PEDOT:PSS/PTB7-Th/CuSCN/Ag. *J–V* characteristics (in a log–log plot) are shown in Fig. S5 of the supplementary material. It shows that a PTB7-Th:$PC_{71}BM$/CuSCN-based hole-only device has an evidently lower current density as compared to that measured for a PTB7-Th/CuSCN-based hole-only device. There is almost no change in the slope of *J–V* curve measured for the PTB7-Th/CuSCN-based hole-only device. However, a distinct hump in the slope of *J–V* curve measured for a PTB7-Th:$PC_{71}BM$/CuSCN-based hole-only device at low voltage is observed, occurred due to the accumulation of space charges in the device.[19] Under illumination, the charge accumulation at the $PC_{71}BM$/CuSCN EBL interface in a double BHJ OPD becomes more prominent due to the trap of the photogenerated charges, thereby producing a photocurrent as a result of the hole tunneling, caused by the band bending in the CuSCN EBL, as shown in Fig. 4(b). For a control OPD, a relatively large noise current can be formed, due to the absence of the interfacial energy barrier at the PTB7-Th/CuSCN EBL, as shown in Fig. 4(c). The schematic diagram of the photocurrent generation in a control OPD under illumination is shown in Fig. 4(d).

Relative photoresponses and cutoff frequency ($f_{-3\ dB}$) of a double OPD and a control OPD, without bias, as a function of frequency of modulated light are shown in Fig. 5(a). $f_{-3\ dB}$, determined by $20\times\log(I/I_0)$, where I is the photocurrent of the OPD generated under

illumination of the modulated light and I_0 is the photocurrent generated by the OPD under illumination of continuous light, is the cutoff frequency of the modulated light at which I reduces to 70.8% of I_0.[14,20] A lower $f_{-3\ dB}$ of 73 kHz was obtained for the double BHJ OPD as compared to that of a control OPD (170 kHz), measured for the OPDs without bias using 50% duty cycled pulsed NIR (1050 nm) LED light source. The response times of the double BHJ OPDs and a control OPD were also measured using an NIR (1050 nm) light source with a modulation frequency of 30 kHz. As shown in Figs. 5(b) and 5(c), the fall time, τ_{fall}, is greater than rise time, τ_{rise}, due to the charge accumulation effect. Therefore, $f_{-3\ dB}$ in an OPD can be more sensitive to its τ_{fall}, e.g., $f_{-3\ dB}=0.35/\tau_{fall}$.[21] The double BHJ OPD has a τ_{fall} of 4.5 μs, yielding an $f_{-3\ dB}$ of 78 kHz using $0.35/\tau_{fall}$ estimation, which agrees well with the measured $f_{-3\ dB}$ of 73 kHz. A relatively slower $f_{-3\ dB}$ of 73 kHz, measured for a double BHJ OPD as compared to that of a control OPD (170 kHz), also reflects the finding of accumulation of photogenerated charges at the $PC_{71}BM$/CuSCN interface, thereby producing a photocurrent because of the hole tunneling effect, caused by the band bending in the CuSCN EBL, as show in Fig. 4(b). The use of a double BHJ results in a notable two orders of magnitude increase in detectivity through a substantial reduction in noise current. The concept of this work demonstrates the advantage and device design freedom of using double BHJ approach for development of high-performance filter-free visible-blind NIR OPDs.

In summary, the performance of visible-blind NIR OPDs was enhanced substantially by incorporating a double BHJ structure. The double BHJ OPDs have a D^* of $>10^{13}$ Jones over the long wavelengths of > 1000 nm, outperforming that of the commercial Si photodetector. The high-performance filter-free visible-blind NIR OPD developed in this work is very encouraging, providing a plethora of applications in areas such as security monitoring, artificial intelligence, high-resolution NIR image sensors, and optical communications.

See the supplementary material for details on material properties, D^* and optical field distribution of a control OPD, and J–V characteristics of hole-only devices.

This work was financially supported by the Research Grants Council, Hong Kong Special Administrative Region, China (12303920 and 12302623), the Guangdong-Hong Kong Technology Cooperation Funding Scheme GHP/121/21GD, the SZ-HK-Macau Science and Technology Plan Project (SGDX20201103095400005), and the Guangdong Basic and Applied Basic Research Fund GDSTC (2022A1515010020).

AUTHOR DECLARATIONS

Conflict of Interest

The authors have no conflicts to disclose.

Author Contributions

The manuscript was written through contributions of all authors.

DATA AVAILABILITY

All data are available within the article or supplementary material.

[1] Z. Lan, M.H. Lee, and F. Zhu, Adv. Intell. Syst. **4**, 2100167 (2021).
[2] B. Siegmund, A. Mischok, J. Benduhn, O. Zeika, S. Ullbrich, F. Nehm, M. Bohm, D. Spoltore, H. Frob, C. Korner, K. Leo, and K. Vandewal, Nat. Commun. **8**, 15421 (2017).
[3] C. Kaiser, K.S. Schellhammer, J. Benduhn, B. Siegmund, M. Tropiano, J. Kublitski, D. Spoltore, M. Panhans, O. Zeika, F. Ortmann, P. Meredith, A. Armin, and K. Vandewal, Chem. Mater. **31**, 9325-9330 (2019).
[4] A. Armin, R.D. Jansen-van Vuuren, N. Kopidakis, P.L. Burn, and P. Meredith, Nat. Commun. **6**, 6343 (2015).
[5] K.W. Tsai, G. Madhaiyan, L.H. Lai, Y.T. Hsiao, J.L. Wu, C.Y. Liao, C.H. Hou, J.J. Shyue, and Y.M. Chang, ACS Appl. Mater. Interfaces. **14**, 38004-38012 (2022).
[6] W. Wang, F. Zhang, M. Du, L. Li, M. Zhang, K. Wang, Y. Wang, B. Hu, Y. Fang, and J. Huang, Nano Lett. **17**, 1995-2002 (2017).
[7] W. Wang, M. Du, M. Zhang, J. Miao, Y. Fang, and F. Zhang, Adv. Opt. Mater. **6**, 1800249 (2018).
[8] B. Xie, R. Xie, K. Zhang, Q. Yin, Z. Hu, G. Yu, F. Huang, and Y. Cao, Nat. Commun. **11**,

2871 (2020).
[9] Z. Lan, L. Cai, D. Luo, and F. Zhu, ACS Appl. Mater. Interfaces. **13**, 981-988 (2020).
[10] S. Xing, X. Wang, E. Guo, H. Kleemann, and K. Leo, ACS Appl. Mater. Interfaces. **12**, 13061-13067 (2020).
[11] Z. Lan, Y. Lei, W.K.E. Chan, S. Chen, D. Luo, and F. Zhu, Sci. Adv. **6**, eaaw8065 (2020).
[12] Z. Lan and F. Zhu, ACS Nano. **15**, 13674-13682 (2021).
[13] J. Kublitski, A. Fischer, S. Xing, L. Baisinger, E. Bittrich, D. Spoltore, J. Benduhn, K. Vandewal, and K. Leo, Nat Commun. **12**, 4259 (2021).
[14] Z. Lan, Y.S. Lau, Y. Wang, Z. Xiao, L. Ding, D. Luo, and F. Zhu, Adv. Opt. Mater. **8**, 2001388 (2020).
[15] Z. Lan, Y.S. Lau, L. Cai, J. Han, C.W. Suen, and F. Zhu, Laser Photonics Rev. **16**, 2100602 (2022).
[16] J. Jiao, Y. Zhang, L. Shi, G. Li, T. Ji, W. Wang, R. Wen, Y. Hao, K. Wang, and F. Zhu, Adv. Opt. Mater. **11**, 2203132 (2023).
[17] K.J. Baeg, M. Binda, D. Natali, M. Caironi, and Y.Y. Noh, Adv. Mater. **25**, 4267-4295 (2013).
[18] X. Ma, H. Bin, B.T. van Gorkom, T.P.A. van der Pol, M.J. Dyson, C.H.L. Weijtens, M. Fattori, S.C.J. Meskers, A.J.J.M. van Breemen, D. Tordera, R.A.J. Janssen, and G.H. Gelinck, Adv. Mater. **35**, 2209598 (2023).
[19] Z. He, X. Du, X. Yu, L. Cao, M. He, J. Han, H. Lin, J. Wang, C. Zheng, and S. Tao, Nano Energy. **114**, 108673 (2023).
[20] F.P. García de Arquer, A. Armin, P. Meredith, and E.H. Sargent, Nat. Rev. Mater. **2**, 1-17 (2017).
[21] S.G. Han, H. Lee, W. Choi, D. Lee, S. Kim, Y. Sung, S. Kim, and K. Cho, Adv. Funct. Mater. **31** (2021).

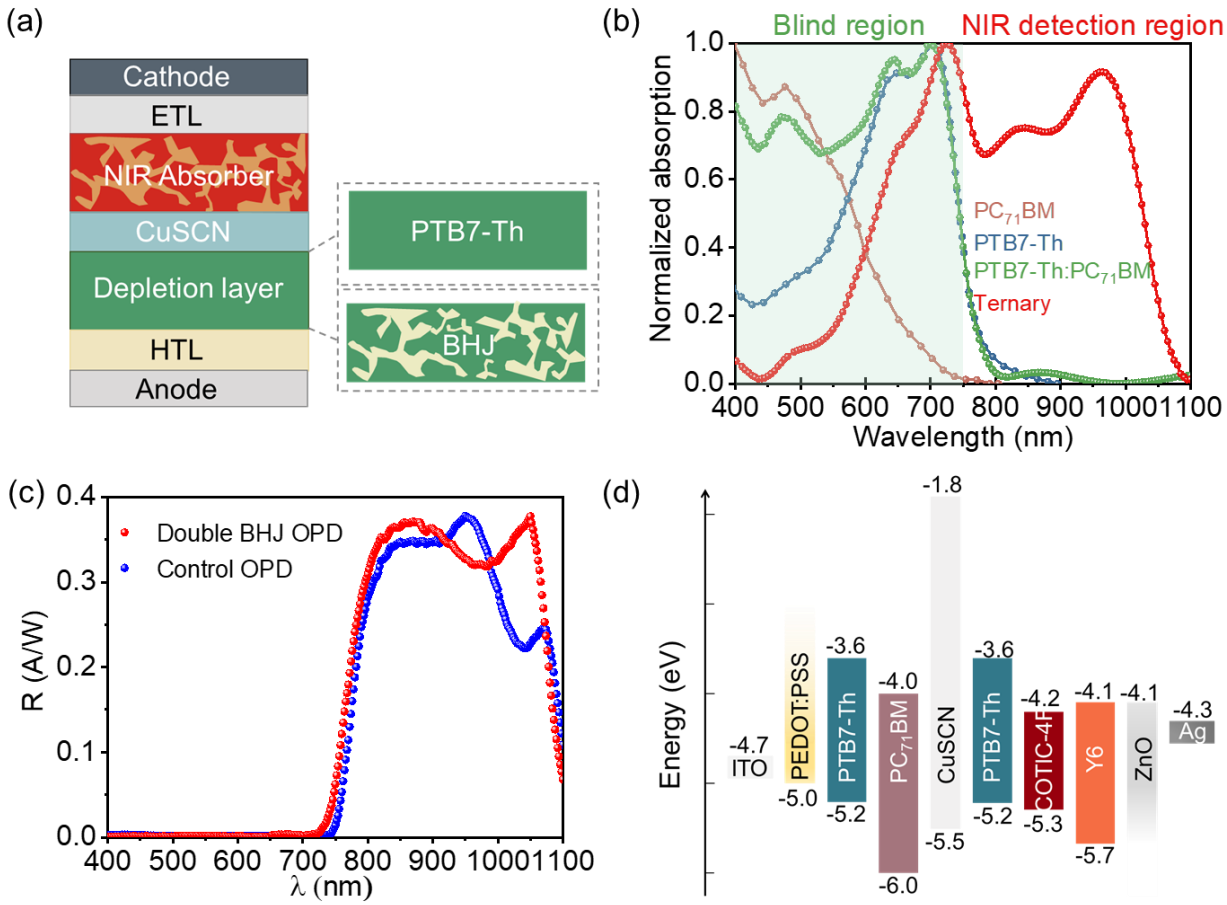

FIG.1. (a) Cross-sectional view of the visible-blind NIR OPDs having different optical depletion layers of PTB7-Th and PTB7-Th:$PC_{71}BM$. (b) Normalized absorption spectra measured for the thin films of $PC_{71}BM$, PTB7-Th, PTB7-Th:$PC_{71}BM$ and PTB7-Th:COTIC-4F:Y6. (c) $R(\lambda)$ obtained for a double BHJ OPD and a control OPD without bias. (d) The schematic diagram showing the energy levels of the functional materials used in the OPDs.

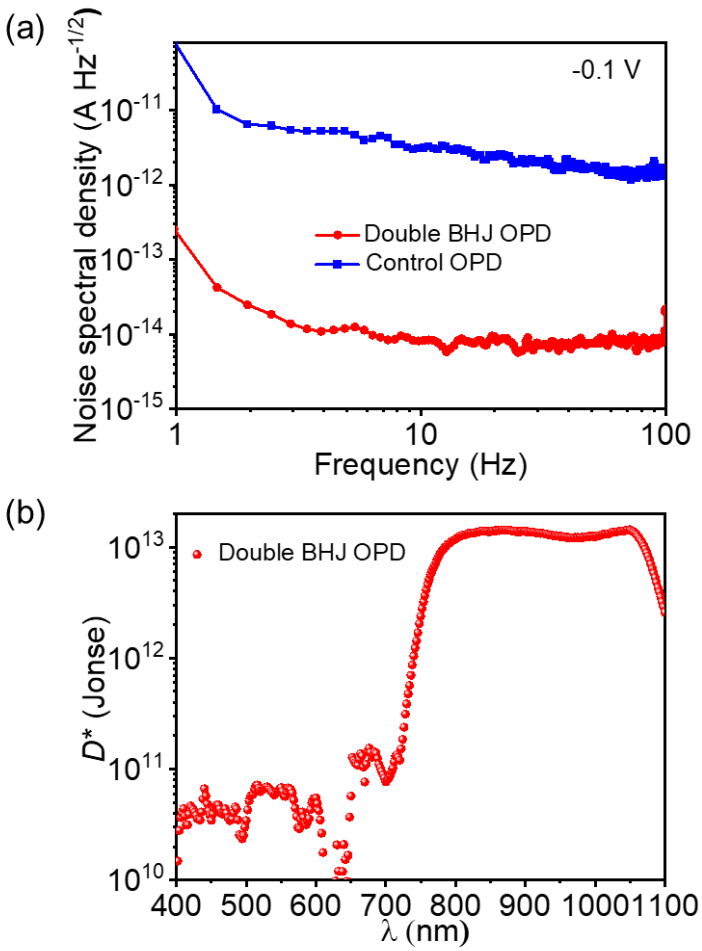

FIG.2. (a) Noise spectral density measured for a double BHJ OPD and a control OPD. (b) D^* obtained for a double BHJ OPD operated at -0.1 V.

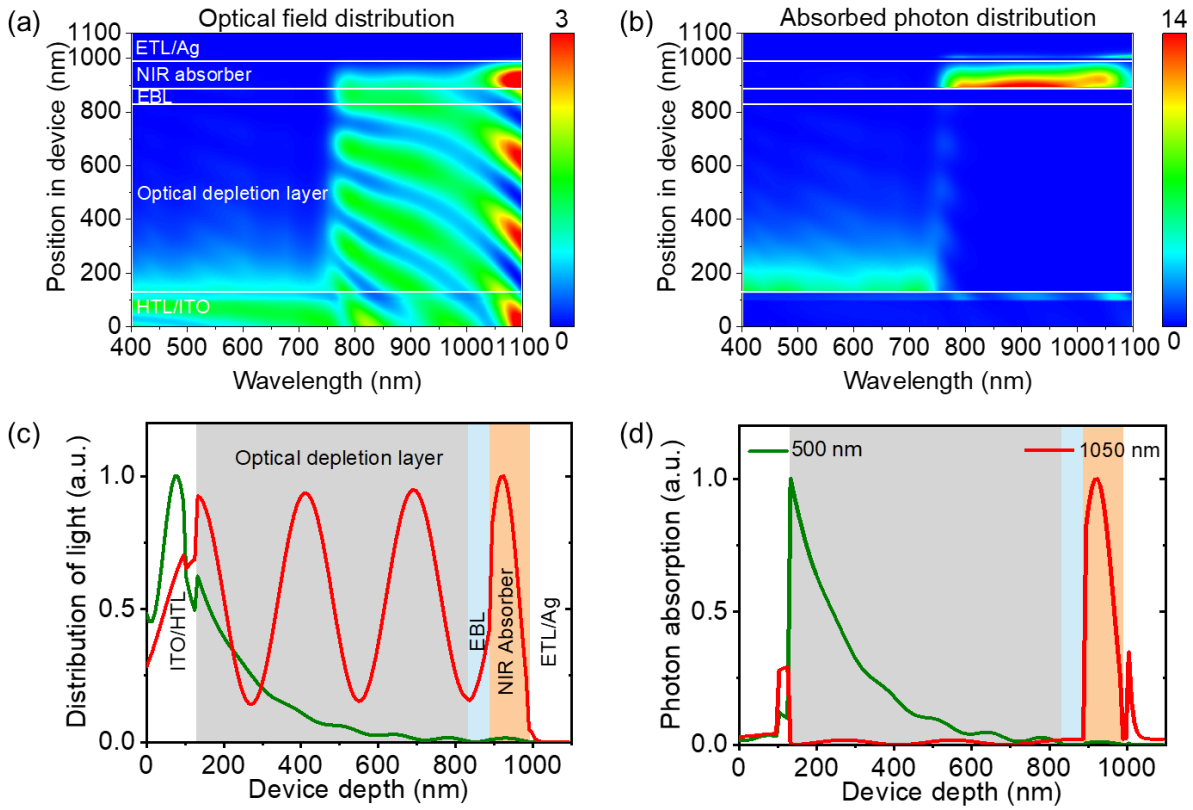

FIG.3. Distribution of (a) optical field and (b) absorbed photon in a double BHJ OPD with a 700 nm thick binary PTB7-Th:$PC_{71}BM$ BHJ optical depletion layer. (c) Optical field distribution and (d) absorbed photon distribution calculated for a double BHJ OPD at 500 and 1050 nm.

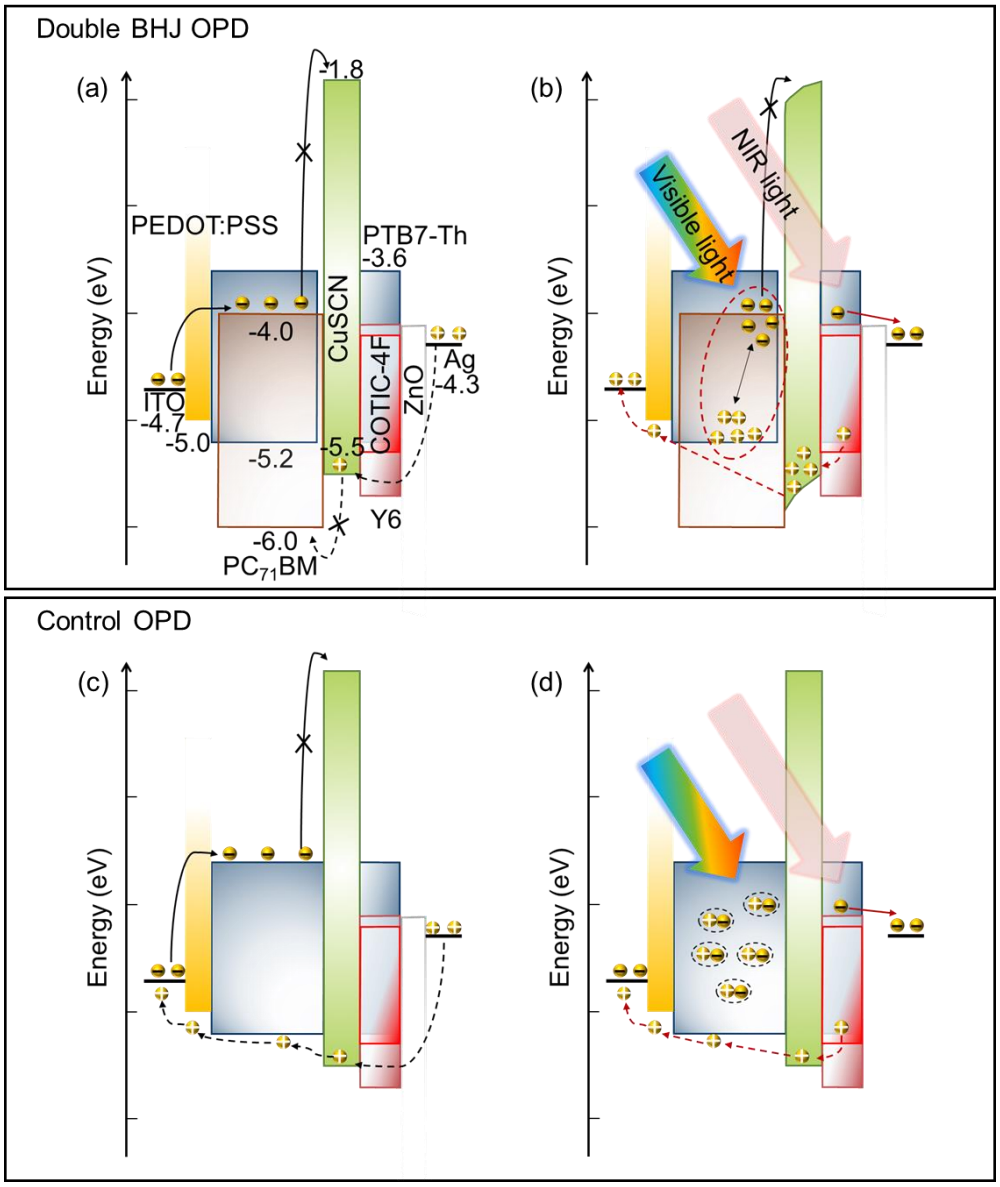

FIG.4. Schematic diagrams illustrate the working principles of a double BHJ OPD: (a) presence of an interfacial energy barrier at the $PC_{71}BM$/CuSCN interface assists in reducing the noise current and (b) accumulation of photogenerated charges at the $PC_{71}BM$/CuSCN interface, producing a photocurrent because of the hole tunneling effect, caused by the band bending in the CuSCN EBL. Schematic diagrams illustrate the working principles of a control OPD: (c) a relatively large noise current formed due to the absence of the interfacial energy barrier and (d) photocurrent generated in a control OPD under illumination.

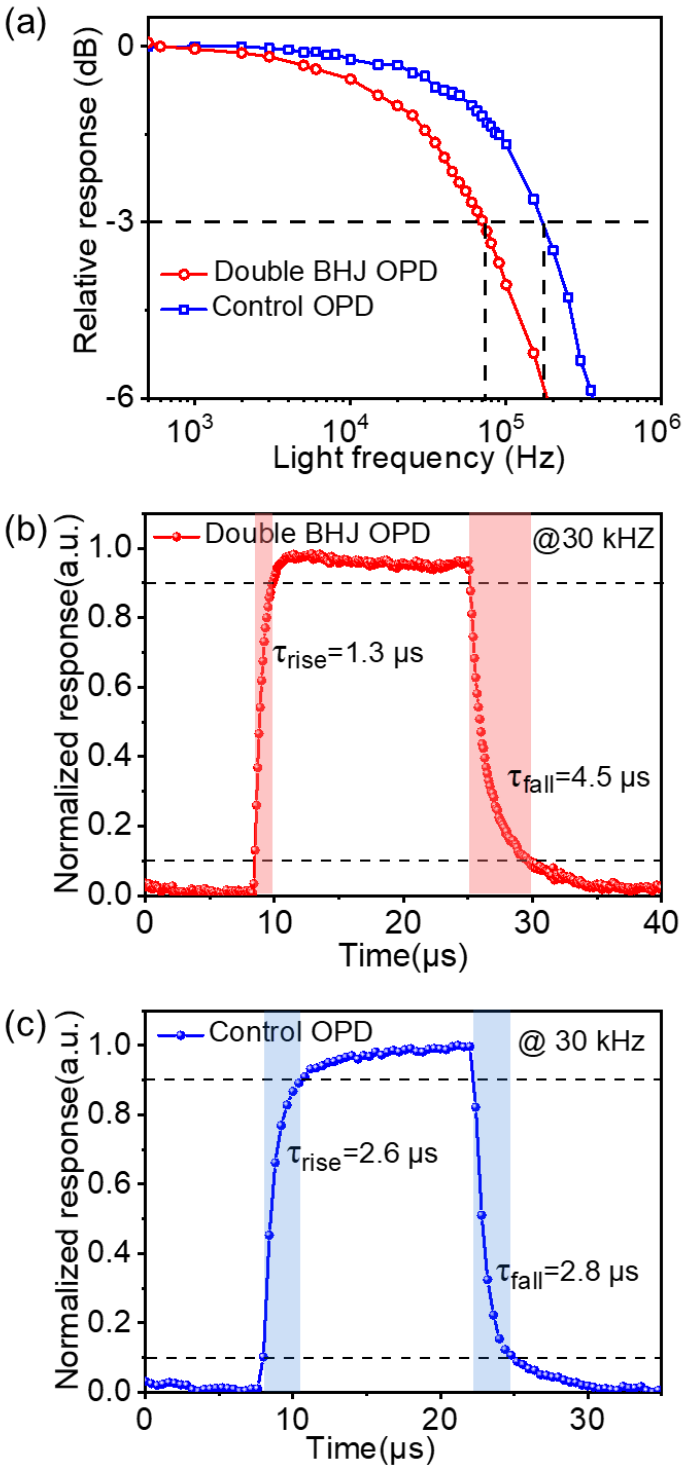

FIG.5. (a) Relative photoresponses measured for a double BHJ OPD and a control OPD, without bias, as a function of frequency of the modulated light (1050 nm) over the frequency range from 1 to 400 kHz. Response time measured for a (b) double BHJ OPD and (c) control OPD.